JOURNAL OF CATALYSIS 148, 270–280 (1994)

ESCA, XRD, and IR Characterization of Aluminum Oxide, Hydroxyfluoride, and Fluoride Surfaces in Correlation with Their Catalytic Activity in Heterogeneous Halogen Exchange Reactions

A. Hess,* E. Kemnitz,* A. Lippitz,† W. E. S. Unger,† and D.-H. Menz‡

*Fachbereich Chemie, Humboldt-Universität zu Berlin, Hessische Straße 1/2, D 10115 Berlin, Germany; †Bundesanstalt für Materialforschung und -prüfung (BAM), Labor 5.33, Gebäude 8.15, Rudower Chaussee 5, D 12489 Berlin, Germany; and ‡Zentrum für anorganische Polymere KAI e.V., Pharm Pur GmbH, Holzweg 27, D 86156 Augsburg, Germany

Received January 28, 1993; revised September 20, 1993

The catalytic activity of certain aluminum oxides, hydroxyfluorides, and fluorides applied to dismutation reactions of the $CHCl_{3-n}F_n$ haloalkane series has been studied. In most cases the catalyst surface has to be modified so that it is catalytically active. A haloalkane flow has been used for the activation procedure. The alteration of the solid phases is followed by XRD and IR. ESCA is applied for the characterization of the solid surfaces before and after treatment with the haloalkanes. As a result of our measurements, we can state that the catalytically active phase which is formed during the activation of the solid samples is stoichiometrically and structurally similar to the β-AlF_3 structure. Using separately synthesized predried β-AlF_3, it could be observed that this sample immediately possess catalytic activity. The nature of the catalytically active species which can be formed using different solid starting substances is discussed. It is possible to draw a correlation between the ESCA results and the catalytic behaviour of a number of solid samples. © 1994 Academic Press, Inc.

INTRODUCTION

Halogen exchange reactions are often initiated by heterogeneous catalysts. A number of metal oxides, hydroxyfluorides, and fluorides (e.g., those of aluminum, chromium, iron, etc.) have been reported to be used as catalysts. However, most of these solid substances have to be activated in a HF or haloalkane flow in order to give sufficient catalytic activity. We have recently published our investigations on these activation processes (1).

This paper characterizes the catalytically active species in the solid surface formed during the activation process. A number of different solid substances are employed as catalyst precursors and the alterations they undergo as a result of reaction with the gas phase are investigated. The correlation between the catalytic activity of the solid sample (determined in a model reaction) and its surface composition is discussed.

The dismutation reactions of the compound $CHClF_2$ are used as a model reaction of the heterogeneously catalyzed halogen exchange

$$2\,CHClF_2 \rightleftharpoons CHCl_2F + CHF_3 \quad \Delta_R G^\circ = -14.5\ \text{kJ/mol} \qquad [1]$$

$$2\,CHCl_2F \rightleftharpoons CHCl_3 + CHClF_2 \quad \Delta_R G^\circ = -14.9\ \text{kJ/mol}, \qquad [2]$$

where the thermodynamic data are from Kauschka and Kolditz (2). We recently published a study regarding the kinetics of this reaction system with an activated γ-Al_2O_3 catalyst (3).

In this paper, a number of structurally different aluminum oxides, hydroxyfluorides, and fluorides are employed as catalysts. In contrast to earlier studies, the processes in the solid phase are of main interest.

METHODS

Apparatus

The investigated solid sample (100 mg, 160–315 μm grain size) was used in a flow reactor. In the case of the preliminary investigations with γ-Al_2O_3, 1 g was used. The drying procedure (3 liter/h nitrogen) was carried out under various adjusted temperature programmes. During the whole time, the amount of HF released by hydrolysis was determined by alkaline absorption. The amount of HF in proportion to the fluoride content of the solid did not exceed 0.2% during the drying process.

After drying, the reactor temperature was set at 625 K and a constant $CHClF_2$ flow (3 liter/h, normal pressure) was adjusted. The composition of the gas phase at the end of the reactor was determined as a function of the

0021-9517/94 $6.00

activation time. Switching on the haloalkane flow defines the activation time $t = 0$. The acid gases contained in the product gas (mainly HCl) were absorbed in a 0.01 mol/liter NaOH solution. In these circumstances a degradation of the haloalkanes does not occur. The chloride content of the solution was determined argentometrically. The fluoride content was analyzed using a fluoride-sensitive lanthanum fluoride electrode. Organic products were analyzed by gas chromatography (column used: Poraplot u, 25 km; detector: FID).

Synthesis and Characterization of Catalysts

The following solid substances were used both as catalysts and as ESCA (XPS) reference samples:

γ-Al_2O_3: commercial; p.a. grade; specific surface area (BET) 180 m^2/g, after drying 210 m^2/g, and after activation 160 m^2/g (surface area does not depend significantly on activation conditions).

β-AlF_3: synthesized by thermal dehydration of α-$AlF_3 \cdot 3H_2O$ according to Ref. (4); specific surface area 31 m^2/g (does not change significantly after drying or activation).

$AlF_{2.3}(OH)_{0.7} \cdot H_2O$: synthesized by boiling a solution of $Al(OH)(CH_3COO)_2$ in a 40 wt.% hydrofluoric acid according to Ref. (5); specific surface area approximately 15 m^2/g (changes during heating).

Further reference samples for ESCA:

α-AlF_3: synthesized by sublimation of technical AlF_3; specific surface area 1 m^2/g;

$Al(OH)_3$ (Bayerite): commercial; p.a. grade; specific surface area 200 m^2/g.

Activation procedure applied to catalysts investigated by ESCA:

γ-Al_2O_3–525 K–$CHClF_2$: dried under N_2-flow (525 K, 30 min), subsequently treated with $CHClF_2$ (3 liter/h, 525 K, 30 min);

γ-Al_2O_3–525 K–CH_3CClF_2: dried under N_2-flow (525 K, 30 min), subsequently treated with CH_3CClF_2 (0.25 liter/h, 525 K, 6 h). For further details about the gas products obtained during the activation with CH_3CClF_2, refer to Ref. (6);

γ-Al_2O_3–675 K–$CHClF_2$: dried under N_2-flow (525 K, 30 min), subsequently treated with $CHClF_2$ (3 liter/h, 675 K, 30 min);

$AlF_2(OH)$-dried: synthesized by drying the $AlF_{2.3}(OH)_{0.7} \cdot H_2O$ sample (295–625 K, 20 K/min, 20 min 625 K, under N_2-flow);

$AlF_2(OH)$–525 K–$CHClF_2$: dried under N_2-flow (295–625 K, 20 K/min, 20 min 625 K), subsequently treated with $CHClF_2$ (3 liter/h, 625 K, 45 min);

β-AlF_3–625 K–$CHClF_2$: dried under N_2-flow (295–625 K, 20 K/min, 20 min 625 K), subsequently treated with $CHClF_2$ (3 liter/h, 625 K, 30 min).

All samples were characterized by X-ray powder diffraction (Cu$K\alpha$ radiation) and infrared spectroscopy (KBr pellet transmission). The determination of the fluoride contents was carried out according to Ref. (7).

Electron Spectroscopy

ESCA measurements were taken with a VG Scientific ESCALAB 200X electron spectrometer. XPS and XAES narrow scan spectra were acquired at Mg$K\alpha$ excitation (15 kV, 20 mA) in FRR mode (CRR 40). The spectrometer energy scale was calibrated employing the procedure and binding energy (*BE*) reference data recommended by Anthony and Seah (8).

XP spectra analysis was performed by peak fitting employing the respective procedures of the VGS 5250 data system. For an estimation of the relative intensities (atomic percentage ratios), we used Scofield's cross sections (9) and a transmission $\sim E_{kin}$. The scatter of these data should be of the order of $\pm 10\%$ at major peaks and at least $\pm 20\%$ when chlorine data are concerned. Let us mention here that when BET surface areas are high, ESCA produces bulk typical data (10). Therefore, we obtained bulk relevant results with the 180 m^2/g γ-Al_2O_3 and the 200 m^2/g $Al(OH)_3$ samples. As regards the low BET surface β-AlF_3 and $AlF_{2.3}(OH)_{0.7} \cdot H_2O$ samples, and the related samples (after drying and/or activation treatments), ESCA "saw" a surface layer which could differ from the bulk seen by XRD and IR.

The sample powders were prepared on standard VG sample stubs with the help of double-sided adhesive film. Before recording spectra, the samples were stored to degas for one night at 10^{-7} mbar within the extended preplock of the ESCALAB. Irradiation of the samples by the X-ray gun increases the pressure within the ion pumped analysis chamber from 1×10^{-10} to $2–3 \times 10^{-9}$ mbar. Due to the preparation, we had to take into account additional XPS C 1*s* signals originating from the adhesive film. Therefore we did not consider the C 1*s* spectrum in the discussion section.

An inner static charge reference is needed to obtain binding or kinetic energy data from an ESCA experiment on poorly conductive samples. In this study we used the aliphatic carbon C 1*s* reference with *BE* = 284.8 eV (11). This approach could be somewhat problematic in the event of heavily coked alumina samples.

RESULTS

Activation of Catalysts

First, γ-Al_2O_3 was employed as a heterogeneous catalyst for the dismutation of $CHClF_2$. Figure 1 shows the

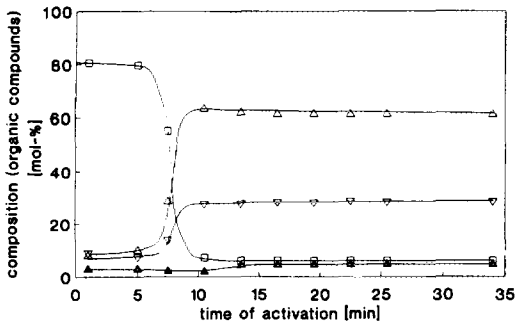

FIG. 1. Change of composition of organic gas phase during the activation of γ-Al_2O_3 with $CHClF_2$ (3 liter/h, T = 525 K, 1 g catalyst, dried under N_2 flow, 30 min, 525 K). (▽) $CHCl_3$, (▲) $CHCl_2F$, (□) $CHClF_2$, and (△) CHF_3.

change of composition of the organic gas phase during the activation process. After approximately 7 min the conversion suddenly increases. At the same time a maximum of released acid gases (>99% HCl, <1% HF) is obtained. Obviously, this alteration of reactivity corresponds to the change from a pure oxide/hydroxide into a partially fluorinated solid surface. This modification of the solid substance is made possible by the degradative reactions of the haloalkanes. The following products are formed: fluoride in the solid substance, HCl, CO, and higher chlorinated haloforms in the gas phase (cf. Ref. (1)).

FTIR spectroscopic studies of the pyridine adsorbates (12) reveal that the surface bridging oxygen is protonated. Brønsted sites have formed. On the other hand, the strength and the amount of the Lewis acid sites have dramatically increased. β-AlF_3 and α-Cr_2O_3 do not exhibit Brønsted sites after activation. We therefore conclude that the catalytic activity depends essentially on the Lewis acidity (12).

Activation procedures of γ-alumina at temperatures up to approximately 525 K do not form new XRD detectable phases. Since the fluoride content exceeds 14 wt.%, it is obvious that phases containing XRD amorphous fluoride are present.

In contrast, XRD reveals the following new phases after activation at 675 K: β-AlF_3 (ASTM 31-11), traces of α-AlF_3 with low crystallinity and large amounts of $AlF_2(OH)$ pyrochlore structure (ASTM 11-631). The infrared spectrum reveals a very high F/OH ratio, since the Al–OH band which is typical for pure $AlF_2(OH)$ is not observed. Probably it is an AlF_3 stoichiometry in a pyrochlore structure. Unreacted γ-Al_2O_3 was also observed. The observation of several resultant fluoride phases led to the idea to synthesize them separately and employ them for comparable activation processes in order to characterize the catalytic behaviour of these phases. Figs. 2a–c show the activation of β-AlF_3 samples. These samples were predried under various temperature conditions. Different times of reactivity change are observed.

As can be concluded from Fig. 2c, it is obvious that after a mild removal of moisture by a linear temperature programme, the sample immediately catalyzes the dismutation without preactivation of its surface. In contrast to Fig. 2c, Fig. 2a shows that the absence of a predrying process results in a different behavior. The moisture must first be removed by reaction with the haloalkanes before catalysis can occur. Previous studies on γ-Al_2O_3 (13) revealed a behaviour which differs from that of β-AlF_3. Independently of any predrying process, this oxide must be activated by the haloalkane flow to develop catalytic activity. Therefore, it can be concluded that a F/OH substitution is required.

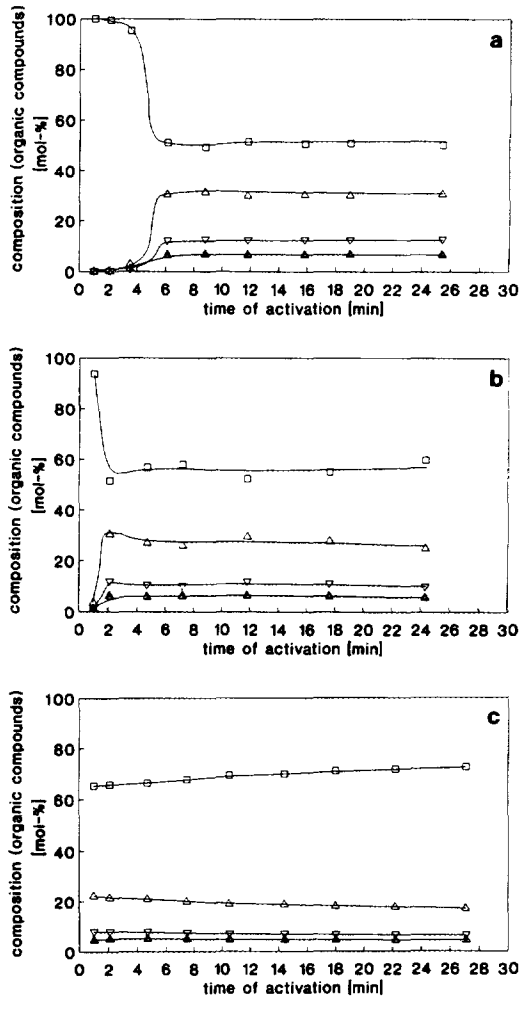

FIG. 2. Change of composition of organic gas phase during the activation of β-AlF_3 with $CHClF_2$ (3 liter/h, T = 625 K, 100 mg catalyst) under different drying conditions. (▽) $CHCl_3$, (▲) $CHCl_2F$, (□) $CHClF_2$, and (△) CHF_3. (a) Without drying; (b) 20 min at 625 K under N_2-flow; (c) 295–625 K, 20 K/min, then 20 min 625 K, under N_2-flow.

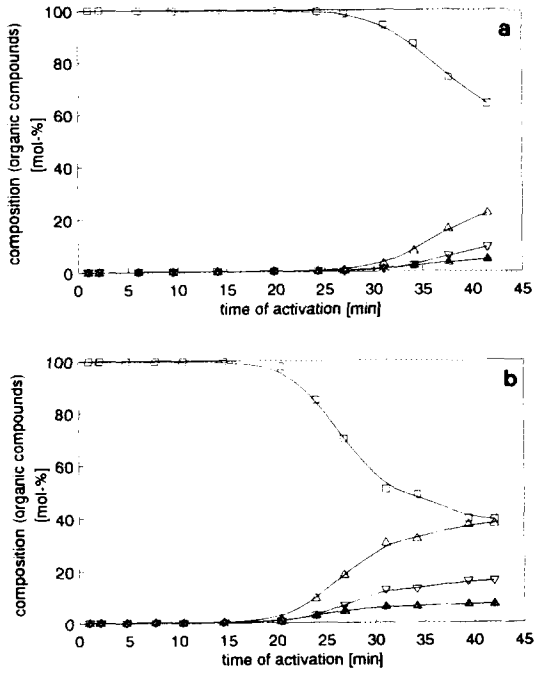

FIG. 3. Change of composition of organic gas phase during the activation of $AlF_{2.3}(OH)_{0.7} \cdot H_2O$ with $CHClF_2$ (3 liter/h, T = 625 K, 100 mg catalyst) under different drying conditions. (▽) $CHCl_3$, (▲) $CHCl_2F$, (□) $CHClF_2$, and (△) CHF_3. (a) Without drying; (b) 295–625 K, 20 K/min, then 20 min 625 K, under N_2-flow.

The compound $AlF_{2.3}(OH)_{0.7} \cdot H_2O$ shows a behaviour similar to that of γ-Al_2O_3 (Figs. 3a,b). From the beginning this compound does not show catalytic activity. This behaviour is independent of the drying processes. The structure contains water in its void spaces (14) which is gradually released, accompanied by a lattice contraction. As long as this water is contained, the solid does not show catalytic activity. After drying, ESCA reveals a partially fluorinated phase together with an oxide phase. This oxide phase is fluorinated during the activation.

Electron Spectroscopy

Reference samples. For a better understanding of the effects of an activation treatment carried out with alumina or aluminum fluorides and hydroxyfluorides, we analyzed XRD-defined reference samples.

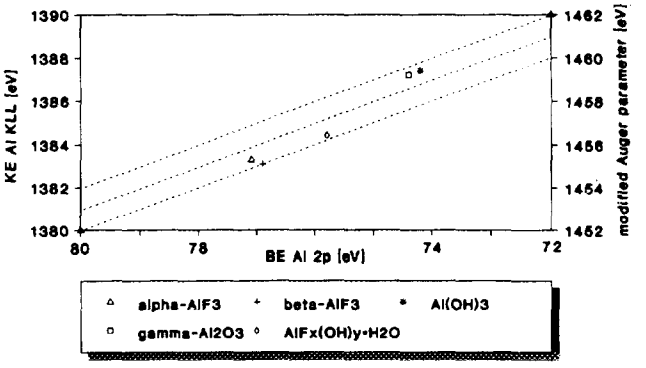

FIG. 4. Chemical state plot for presentation of ESCA data obtained for Al with reference γ-alumina and Al fluoride and hydroxyfluoride samples. (Static charge reference C 1s = 284.8 eV.)

Table 1 presents spectroscopic data obtained for the unresolved Al 2p doublet, the Al 2s and F 1s photo peaks, the F $KL_{23}L_{23}$ and the Bremsstrahlung-induced Al $KL_{23}L_{23}$ Auger electron emission peaks, and the modified Auger parameters α'. These data are summarized in chemical state plots following Wagner and Joshi (15) in Figs. 4 and 5. In a chemical state plot, the kinetic energies (*KE*) of Auger electrons are on the ordinate, whereas the *BE* of the photo peaks are on the abscissa. The α' grid is drawn as a family of parallel lines with a slope of 1. All points on any one of these lines have the same modified Auger parameter. The advantage of presenting data this way is that each well defined chemical state occupies a unique position on the two-dimensional grid, thus giving the possibility of finger printing.

Considering Figs. 4 and 5 we found the $Al(OH)_3$- and γ-Al_2O_3-related points at very similar positions within the chemical state plot for Al. Obviously, the aluminum hydroxyfluoride-related data points are well separated. The α- and β-AlF_3-related data points were also found at similar positions, also well separated from that of the hydroxyfluoride. Considering the F chemical state plot, the aluminum fluorides and hydroxyfluoride are repre-

TABLE 1

Detailed XPS and XAES Al and F Data Obtained with Reference Samples (Static Charge Reference: C 1s = 284.8 eV)

Sample	*BE* Al 2p/FWHM [eV]	*BE* Al 2s/FWHM [eV]	*KE* Al KLL [eV]	α'_{Al}[a] [eV]	*BE* F 1s/FWHM [eV]	*KE* F KLL [eV]	α'_F [eV]
γ-Al_2O_3	74.4/2.7	119.5/3.2	1387.2	1461.6			
$Al(OH)_3$ bayerite	74.2/2.1	119.6/2.6	1387.4	1461.6			
α-AlF_3	77.1/3.0	122.0/3.0	1383.3	1460.4	687.5/2.8	652.3	1339.8
β-AlF_3	76.9/3.0	121.8/3.5	1383.1	1460.0	687.8/3.0	651.7	1339.5
$AlF_{2.3}(OH)_{0.7} \cdot H_2O$	75.8/2.6	120.7/3.0	1384.4	1460.2	687.0/2.8	652.6	1339.6

[a] Evaluated with *BE* Al 2p.

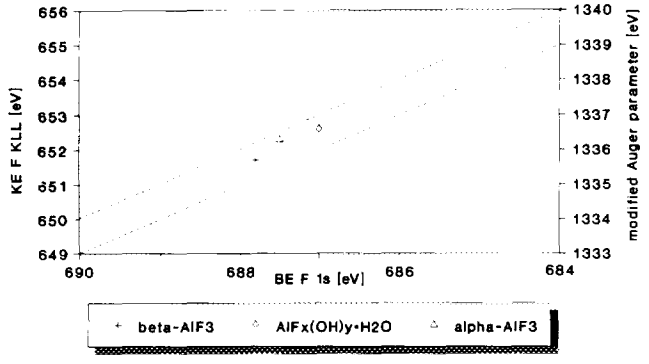

FIG. 5. Chemical state plot for presentation of ESCA data obtained for F with reference Al fluoride and hydroxyfluoride samples. (Static charge reference C 1*s* = 284.8 eV.)

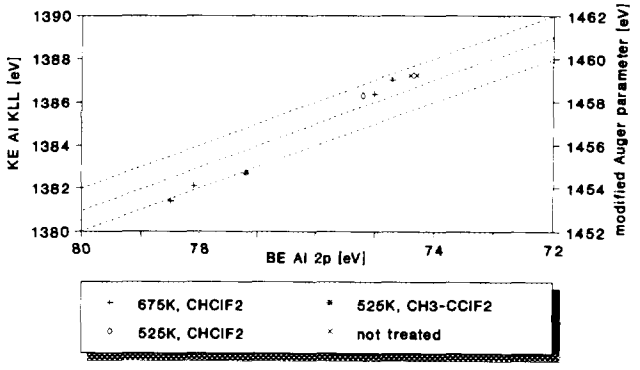

FIG. 6. Chemical state plot for presentation of ESCA data obtained for Al with γ-alumina activated with fluorochlorohydrocarbons at different temperatures. (Static charge reference C 1*s* = 284.8 eV.)

sented by points scattered over a certain field with the fluorides occurring at lower *KE*s and higher *BE*s. Relevant Al and F literature data are presented in Table 2 for comparison. Reliable data are hard to find, especially in the case of F.

Considering the O 1*s* photo peaks (see Table 3), we found a single species with γ-Al_2O_3 and $Al(OH)_3$ at *BE* = 531.9 eV and 532.1 eV, respectively. With the fluorides and the hydroxyfluoride, we found two species in each case, a major one at BE ≈ 533 eV and another at ≈ 535 eV. It seems that the surface region of the fluorides was not fully free of water and OH^--groups. However, the total oxygen content of the surface of α- and β-AlF_3 was rather small in comparison to the hydroxyfluoride.

Activated γ-alumina. Spectroscopic Al and F related data are given in Table 4. These data are also presented in chemical state plots (cf. Figs. 6 and 7). The alterations of the total F, O, and Cl content of the investigated alumina sample in the course of an activation procedure are recorded in Figs. 8 and 9.

Activation of γ-alumina with $CHClF_2$ at 525 K results in a position shifted towards the aluminum hydroxyfluoride position within the Al chemical state plot. The position

TABLE 2

Relevant Spectroscopic Reference Al and F Data from the Literature

Sample/charge reference	*BE* Al 2*p* [eV]	*BE* Al 2*s* [eV]	*KE* Al KLL [eV]	α'_{Al} [eV]	*BE* F 1*s* [eV]	*KE* F KLL [eV]	α'_F [eV]	Ref.
γ-Al_2O_3/C 1*s* = 284.6 eV	73.52		1388.03	1461.55				16
$Al(OH)_3$, bayerite/C 1*s* = 284.6 eV	73.70		1387.82	1461.52				16
AlF_3				1460.7				16
Al_2O_3/C 1*s* = 285.0 eV	74.3						1340.5	17
AlF_3/C 1*s* = 285.0 eV	77.0						1339.9	17
Na_32AlF_6/C 1*s* = 285.0 eV	76.0						1339.7	17
AlF_3/C 1*s* = 285.0 eV	76.5	121.2						18
$Al(OH)_3$, bayerite/Au $4f_{7/2}$ = 83.0 eV	74.7							19
$Al(OH)_3$, bayerite/C 1*s* = 285.0 eV	74.5		1387.5	1462.0				20
γ-Al_2O_3/C 1*s* = 284.8 eV	74.2							21
γ-Al_2O_3/Au $4f_{7/2}$ = 84.0 eV	74.3							22
AlF_3				1460.7				23
$AlF_3 \cdot 3H_2O$/C 1*s* = 284.8 eV					686.3			24
Fluorinated graphite, C_4F					687.2	656.7	1343.9	25
Fluorinated graphite, CF					689.2	653.1	1342.3	25
High fluorinated fluorographites/C 1*s* = 285.0 eV					~690.5			26
Low-temperature fluorographites/C 1*s* = 285.0 eV					~689.0			26
Conductive low-temperature fluorinated graphite					685.7			27
"F_2 adsorbed on graphite"					687.5–689.0			27

TABLE 3

Oxygen XPS Data Obtained with Reference Samples and Treated Samples (Static Charge Reference: C 1*s* = 284.8 eV)

Sample	*BE* O 1*s* [eV] (rel. int. (%))				
	535	534	533	532 Hydroxide	532 Oxide	531
γ-Al_2O_3			533.6(8)		531.9(92)	
$Al(OH)_3$ bayerite					532.1(100)	
α-AlF_3		534.3(35)		532.4(65)		
β-AlF_3	535.3(21)		533.5(79)			
$AlF_{2.3}(OH)_{0.7} \cdot H_2O$		534.6(14)	533.3(86)			
γ-Al_2O_3–525 K–$CHClF_2$			533.4(19)		532.0(81)	
γ-Al_2O_3–525 K–CH_3CClF_2		534.1(100)				
γ-Al_2O_3–675 K–$CHClF_2$	535.4(4)		533.4(25)		531.9(71)	
β-AlF_3–625 K–$CHClF_2$		534.0(100)				
$AlF_2(OH)$-dried			533.5(80)		531.8(20)	
$AlF_2(OH)$–625K–$CHClF_2$		534.1(100)				

of these samples within the F chemical state plot is far from those observed with fluorides or hydroxyfluorides of Al. The O/Al intensity ratio significantly decreases due to the activation. There is a slight uptake of F and a very slight uptake of Cl. The Cl 2*p* photo peak was measured with a *BE* > 199 eV, suggesting that Cl is part of chlorine organic species (cf. Ref. (11)).

Activation of γ-alumina with CH_3–$CClF_2$ (cf. Ref. [6]) at 525 K gives different results. The position of this sample within the Al and F chemical state plot is almost identical with those obtained with our AlF_3 reference samples. The O/Al intensity ratio is strongly diminished, whereas the F/Al intensity ratio reaches a value also observed with pure AlF_3. A slight uptake of Cl occurs where the Cl 2*p* *BE* is once again measured with *BE* > 199 eV. Activation of γ-alumina in $CHClF_2$ at 675 K results in ESCA spectra (cf. Fig. 10), suggesting the existence of two F and two Al species. Looking at the Al chemical state plot we found one Al majority (~75%) species with spectroscopic parameters very similar to those observed with Al in γ-alumina treated with $CHClF_2$ at 525 K. The second (minority) Al species is found at a position which was not reached with our reference samples (lower *KE* and higher *BE* than measured with AlF_3). Considering the F chemical state plot we found the majority (~75%) F species at a position clearly different from that obtained for Al fluorides (higher *BE* and lower *KE*). However, there was a considerable scatter with the F data in this study. In Fig. 6, the results of two independent measurements with the sample under consideration are indicated. The relative intensity of oxygen decreases due to the fact that activation is very similar to the situation encountered in the

TABLE 4

Detailed XPS and XAES Al and F Results Obtained with Treated Alumina, Aluminum Fluoride, and Hydroxyfluoride (Static Charge Reference: C 1*s* = 248.8 eV)

Sample/treatment	*BE* Al 2*p*/FWHM [eV]	*BE* Al 2*s*/FWHM [eV]	*KE* Al KLL [eV]	α'_{Al} [eV]	*BE* F 1*s*/FWHM [eV]	*KE* F KLL [eV]	α'_F [eV]
γ-Al_2O_3–525 K–$CHClF_2$	75.2/2.9	120.3/3.3	1386.3	1461.5	686.4/3.0	653.6	1340.0
γ-Al_2O_3–525 K–CH_3CClF_2	77.2/3.1	122.2/3.6	1382.7	1459.9	688.1/3.1	651.4	1339.5
γ-Al_2O_3–675 K–$CHClF_2$	78.1/2.9	123.1/3.2	1382.1	1460.2	689.1/2.9^m	650.7^m	1339.7^m
	74.7/2.7^m	119.8/3.3^m	1387.0^m	1461.7^m	686.6/2.9	653.7	1339.9
β-AlF_3–625 K–$CHClF_2$	76.8/2.5	121.8/2.9	1383.1	1459.9	687.9/2.4	651.6	1339.5
$AlF_2(OH)$-dried	76.2/2.6^m	121.2/3.0^m	1384.0^m	1460.2^m	687.5/2.5	652.2	1339.7
	74.8/2.6	119.8/2.9	1386.4	1461.2			
$AlF_2(OH)$–625 K–$CHClF_2$	77.0/3.1	121.9/3.4	1383.0	1460.0	687.9/3.0	651.6	1339.5

Note. superscript m, majority species.

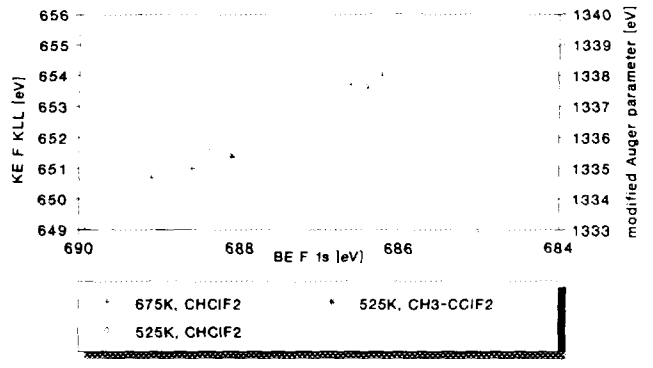

FIG. 7. Chemical state plot for presentation of ESCA data obtained for F with γ-alumina activated with fluorochlorohydrocarbons at different temperatures. (Static charge reference C 1*s* = 284.8 eV.)

sample activated at 525 K in $CHClF_2$. A medium Al-related uptake of F has to be noted, whereas the uptake of Cl reaches its maximum (Cl/Al atomic percentage ratio ~0.07) at these alumina activation conditions. As before, Cl should be part of chlorine organic species.

Activated β-AlF_3. Activation of β-AlF_3 in $CHClF_2$ at 525 K gives no significant alterations of the F/Al and O/Al intensity ratios and the spectroscopic parameters obtained for Al and F (cf. Tables 1 and 4, Fig. 8). A small organic bound uptake of Cl was observed.

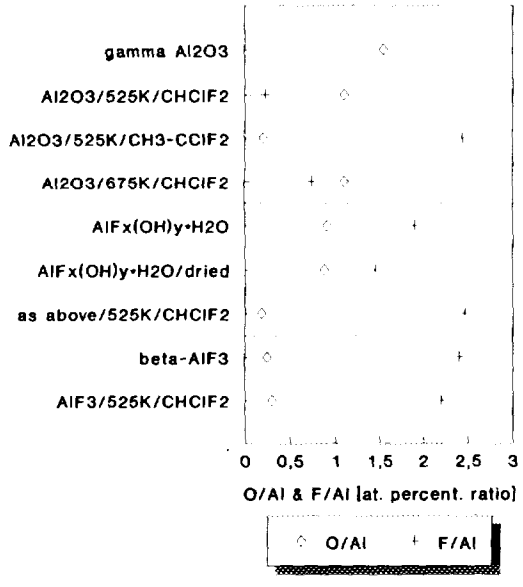

FIG. 8. Relative intensities obtained from corrected XPS O 1*s*, F 1*s*, and Al 2*s* intensities with γ-alumina before and after activation, $AlF_{2.3}(OH)_{0.7} \cdot H_2O$ before and after drying and activation, and β-AlF_3 before and after activation with fluorochlorohydrocarbons at different temperatures.

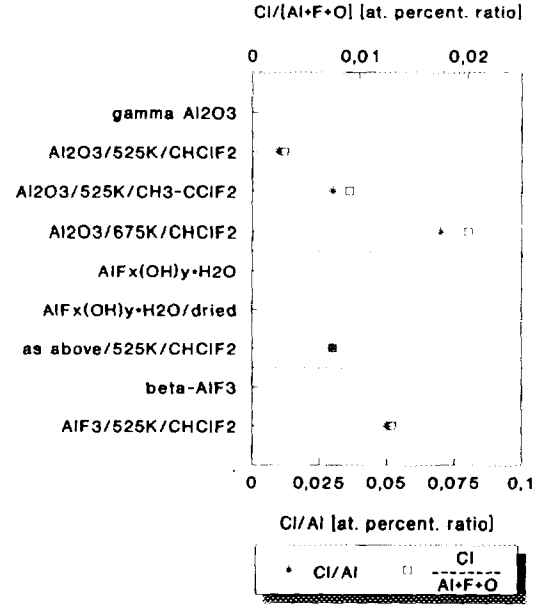

FIG. 9. Relative intensities obtained from corrected XPS Cl 2*p*, F 1*s*, and Al 2*s* intensities with γ-alumina before and after activation, $AlF_{2.3}(OH)_{0.7} \cdot H_2O$ before and after drying and activation, and β-AlF_3 before and after activation with fluorochlorohydrocarbons at different temperatures.

Drying and Activation of $AlF_{2.3}(OH)_{0.7} \cdot H_2O$. Drying of $AlF_{2.3}(OH)_{0.7} \cdot H_2O$ in a N_2-stream at 625 K results in the formation of two Al surface species. Figure 11 shows distinct shoulders on the low *BE* side of the Al 2*p* photo peak and on the high *KE* side of the main peak of the Al $KL_{23}L_{23}$ Auger signal. Table 4 presents the relevant spectroscopic data for F and Al which are summarized in the respective chemical state plots (cf. Figs. 12 and 13). The Al minority species (~20%) is observed with a position in the chemical state plot close to that of pure γ-alumina, whereas the majority species occurs at a position almost identical to this characteristic of $AlF_{2.3}(OH)_{0.7} \cdot H_2O$. In the F chemical state plot we observe a clear drying-related shift of the respective position towards the positions of the AlF_3 samples. It is somewhat surprising that there is no significant decrease of the O/Al intensity ratio (cf. Fig. 8). On the other hand we observed an alteration of the O 1s spectrum (cf. Table 3). The species at *BE* = 534.6 eV disappeared, the species at *BE* ≈ 533 eV represents the majority (80%), and another species at *BE* = 531.8 eV appears. Activation of this sample using $CHClF_2$ at 525 K results in the formation of only one Al species with a position in the chemical state plot unequivocally the same as observed with our Al fluorides. Considering the F species, we have to state that its position in the chemical state plot agrees with those observed with our β-AlF_3. Al-related Cl uptake

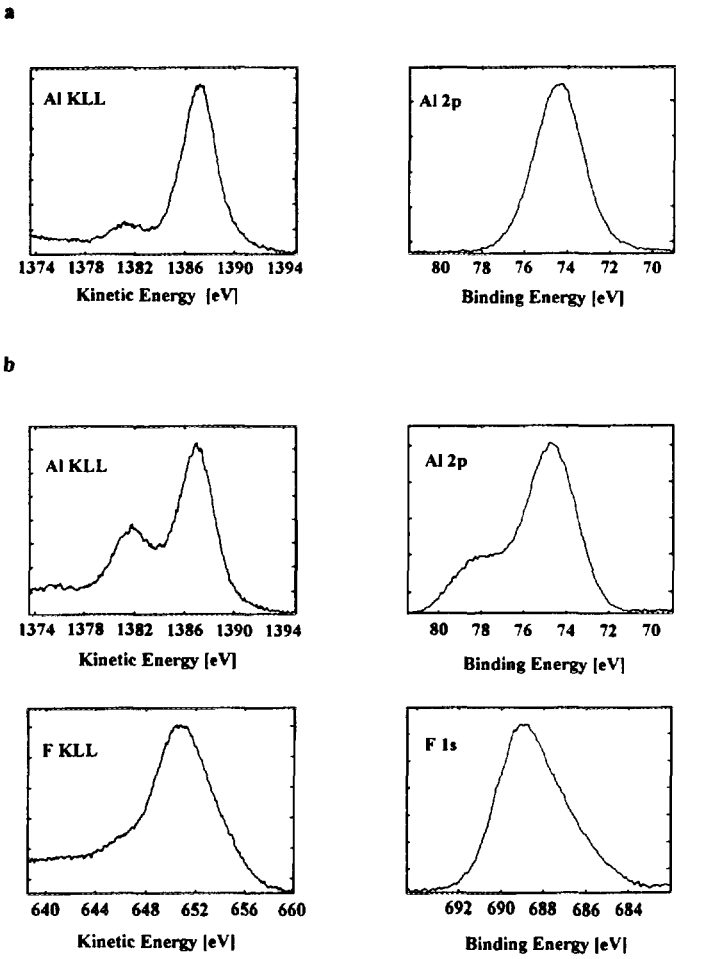

FIG. 10. Intensities of Al XPS and XAES narrow scans obtained with (a) γ-Al_2O_3 in the "as-received" state and Al and F XPS and XAES narrow scans obtained with (b) γ-Al_2O_3 after activation with $CHClF_2$ at 675 K. Note the occurrence of a second minority peak on the high *BE* side of Al 2*p*, the corresponding change within the Al KLL Auger spectrum and the special shape of the F 1*s* and F KLL spectra, suggesting the existence of more than one F species in (b).

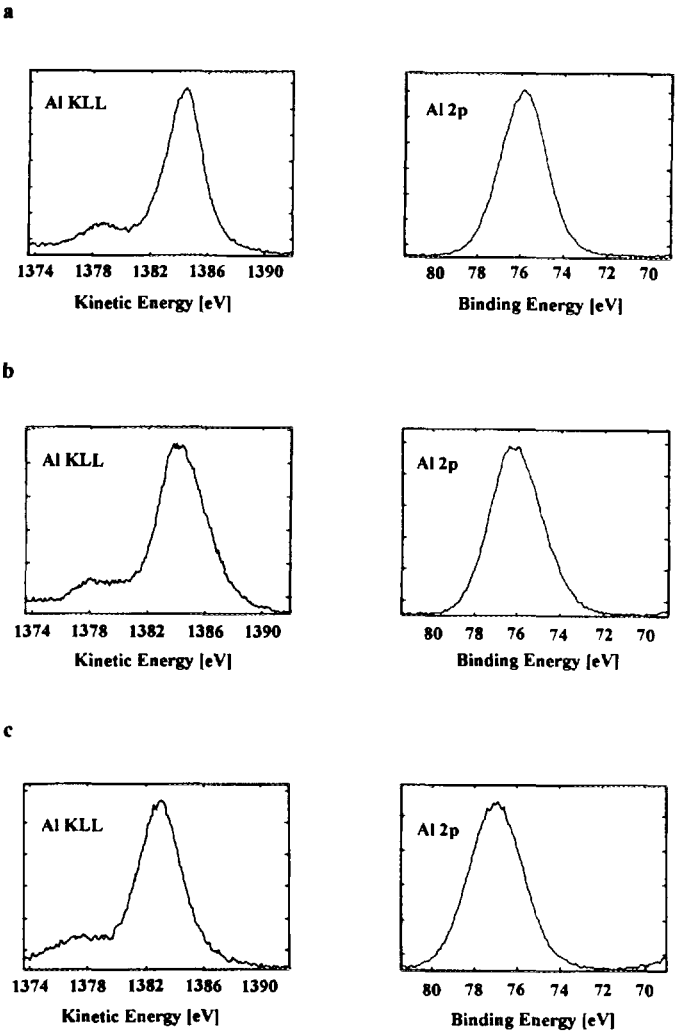

FIG. 11. Intensities of Al XPS and XAES narrow scans obtained with $AlF_{2.3}(OH)_{0.7} \cdot H_2O$ (a) in the "as-received" state, (b) after drying this sample in N_2 and (c) after subsequent activation with $CHClF_2$. Note the occurrence of Al 2*p* *BE* and Al KLL *KE* shifts after activation treatment and the peak shapes obtained after drying, suggesting the existence of a second minority Al species (shoulder on the low *BE* side of the Al 2*p* peak).

(organic chlorine species) is small, whereas the F/Al ratio reaches the value characteristic of untreated β-AlF_3 (cf. Figs. 8 and 9).

DISCUSSION

The Concept of the Auger Parameter

At this point we briefly restate the concept of the Auger parameter for a discussion of electron spectroscopy data. Wagner's original definition (cf. Ref. (15)) of α was

$$\alpha = KE(\text{Auger electron}) - KE(\text{photo electron}). \quad [3]$$

With $h\nu = KE(\text{photo electron}) + BE(\text{photo electron})$ one obtains the definition of the modified Auger parameter

$$\alpha' = \alpha + h\nu = KE(\text{Auger electron}) + BE(\text{photo electron}). \quad [4]$$

In an approximation introduced by Wagner (28) and Thomas (29), the energy shifts, usually observed in a comparison of ESCA results obtained with different chemical states of an element, can be analyzed in terms of initial state and final state contributions,

$$\delta BE = \delta V - \delta R, \quad [5]$$

$$\delta KE = -\delta V + 3\delta R \quad [6]$$

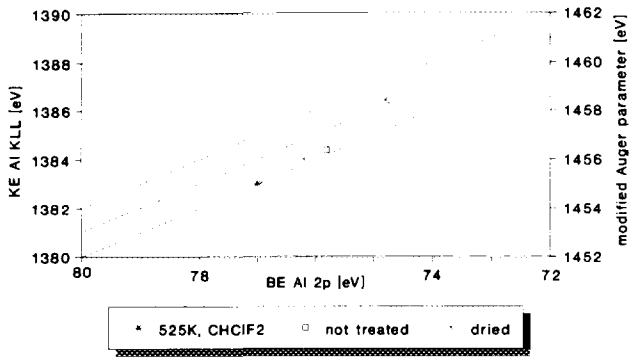

FIG. 12. Chemical state plot for presentation of ESCA data obtained for Al with $AlF_{2.3}(OH)_{0.7} \cdot H_2O$ dried in N_2 and activated with $CHClF_2$. (Static charge reference C 1*s* = 284.8 eV.)

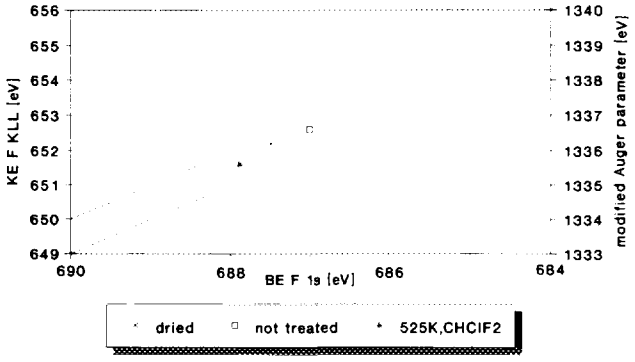

FIG. 13. Chemical state plot for presentation of ESCA data obtained for F with $AlF_{2.3}(OH)_{0.7} \cdot H_2O$ dried in N_2 and activated with $CHClF_2$. (Static charge reference C 1*s* = 284.8 eV.)

and

$$\delta\alpha' = \delta BE + \delta KE = 2\delta R, \qquad [7]$$

where δV reflects the alteration of an initial-state charge distribution on the atom undergoing photoionization and δR is the extra-atomic relaxation energy. The latter characterizes the change of screening of a final core hole state in the emitting atom by polarization of its ligands. A comparison is made between atoms in rather similar environments and nonlocal screening occurs (cf. discussion in Ref. (30)). Equations [5] and [7] are useful for a more detailed interpretation of ESCA data.

As regards the structure of the reference samples investigated in this study, we can state that oxide,[1] hydroxide, or fluoride ions lie at the corners of regular octahedra with Al ions arranged in the centers. The relevant Al–O, $Al–O_{OH}$, and Al–F distances are also similar (14, 31). Following the given approach we find no difference in δR and only a small one in δV when Al_2O_3 and $Al(OH)_3$ are compared. Comparison of Al_2O_3 with the hydroxyfluoride and the fluoride samples reveals for Al an overall decrease of the relaxation energy by ~0.7 eV and an increase in the initial-state potential effect δV by ~0.7 and ~1.9 eV, respectively. Hence it follows (as is to be expected from a chemical point of view) that the ionicity of the Al–ligand bond increases while going from alumina to Al fluoride, whereas the parallel decrease in polarizability results in a loss of screening of an Al 2*p* core hole.

Activated γ-Alumina

Activation with $CHClF_2$ at 525 K results in a single Al species characterized by an unchanged modified Auger parameter and a small enhancement of the initial-state potential effect (≤1 eV). XRD revealed that no crystalline phases were formed. The conclusion is that this Al species should be a precursor for the formation of an Al (hydroxy)fluoride. Considering the trend of F ESCA data (cf. Fig. 9, exchange of OH^- with F^- results in an increase of the F 1*s* *BE* at constant modified Auger parameter) one could speculate that, on a few sites of the γ-alumina, OH^- is statistically exchanged with F^- in the course of activation. This exchange is accompanied by a charge transfer from Al to F atoms. This results in an increase of Lewis acidity and therefore in an increase of the catalytic activity (cf. Fig. 1).

Finally, one should estimate the existence of a chemisorbed $C_kH_lCl_mF_n$ overlayer on the alumina, e.g., fluorinated (and chlorinated) coke. We refer here to the fact that the chlorine observed by ESCA is part of an organic substance and that Palchan *et al.* (27) reported a low F 1*s* *BE* of 685.7 eV with low temperature fluorinated graphite.

It is assumed that the $C_kH_lCl_mF_n$ overlayer is the product of the degradative side reactions of the haloalkanes. This overlayer is the precursor of the observed coke. Here it cannot be excluded that the organic layer has an influence on the catalytic mechanism (cf. Ref. (32)).

Activation with $CHClF_2$ at 675 K results in a rather complex multiphase sample. ESCA "saw" a majority Al species with data very similar to those measured with the sample γ-Al_2O_3–525 K–$CHClF_2$ (cf. discussion above). A second minority Al species was found at the same α' value as Al fluorides or hydroxyfluorides but with substantially higher (roughly 1 eV) *BE*. Bearing in mind that F is the most electronegative ligand of all, the initial-state potential effect δV on Al provided by six octahedrally coordinated F atoms cannot be exceeded. XRD also revealed an octahedral pyrochlore $Al(OH)F_2$ together with a β-AlF_3 phase with this activated γ-Al_2O_3 sample, but the typical Al ESCA data of these phases could not be

[1] With the exception of tetrahedral vacancies in γ-alumina, which cannot be resolved by ESCA.

obtained. The signal of the minority Al species is shifted to a higher BE with respect to Al in AlF_3.

A similar problem arises in regard to the two F species revealed by ESCA analysis. The majority species was found with an α' value characteristic of a fluoride but the F 1*s* *BE* is higher (by roughly 1.3 eV) than that observed in the fluoride reference samples. The second F species seems to be the same as the one discussed under the γ-Al_2O_3–525 K–$CHClF_2$ sample.

The shift to higher *BE*s observed by ESCA for Al and F with respect to the AlF_3 results could be due to a particle size effect or a support interaction. The octahedral coordination may be disturbed, which would explain the strongly altered relaxation conditions. Finally, we note that the evaluation of the F/Al atomic percentage ratio with the respective data obtained for the strikingly *BE* shifted species gives 2.3, approximately the same value measured with the fluoride reference samples.

The conclusion is that this sample consists most probably of high F/OH ratio Al (hydroxy)fluoride particles and slightly fluorinated alumina both covered by a chlorinated and fluorinated coke layer.

A very long activation in CH_3–$CClF_2$ at 525 K results in a single Al and a single F species. Together they form an Al hydroxyfluoride phase characterized by a F/Al atomic ratio of ~2.5. The long activation procedure results in the disappearance of the signals characteristic of slightly fluorinated alumina.

Activation of Al Fluorides and Hydroxyfluorides

Drying of the hydroxyfluoride sample $AlF_{2.3}(OH)_{0.7} \cdot H_2O$ in N_2 at 625 K results in two coexisting phases at the sample surface. ESCA reveals that the majority one should be very similar to the β-AlF_3 phase prepared as a reference sample. The second phase is without any doubt alumina. A similar result was reported by Fourquet *et al.* (14) for $AlF_{1.5}(OH)_{1.5} \cdot H_2O$. Through thermal analysis and XRD they found a desorption of the water molecules out of the pyrochlore network at 475 K, and, in a second step of dehydration, the disintegration into AlF_3 and Al_2O_3 at 725 K.

After activation of the dried sample in $CHClF_2$ at 525 K, ESCA reveals the disappearance of alumina from the surface and the formation of Al (hydroxy)fluoride with a high F/Al atomic ratio of ~2.5. Figure 3 shows the corresponding course of activation. Obviously, the increase of the catalytic activity corresponds to the change from an alumina-containing surface into a pure Al(hydroxy)fluoride surface of high F/Al ratio. The disintegration product alumina was fluorinated by the haloalkanes.

Activation of the reference sample β-AlF_3 in $CHClF_2$ at 525 K causes no further alteration of the surface and the bulk which could be observed by ESCA or XRD. The catalytic activity behaviour of predried β-AlF_3 is shown in Fig. 2c. It catalyzes the dismutation from the very beginning of the activation procedure.

O 1s Spectra

ESCA data obtained for O 1*s* are shown in Table 3. We restrict our assignment to oxide species (O 1*s* *BE* ≈ 531.5 eV (33)) and hydroxide species (O 1*s* *BE* ≈ 532.5 eV (33)) only. The O 1*s* *BE*s of adsorbed water or of crystal water are not known for our samples. Therefore we cannot assign the O 1*s* signals measured with BEs > 533 eV exactly. Nevertheless, it is remarkable that the activated samples β-AlF_3, $AlF_2(OH)$–525 K–$CHClF_2$, and γ-Al_2O_3–525 K–CH_3CClF_2 reveal comparable single O 1*s* signals at *BE* ≈ 534.2 eV. The following explanation may be proposed. Stronger Lewis acid sites are formed as a result of the activation process. After leaving the reactor, but also during the activation, the sample is subjected to a humidity attack. This should result in an adsorption of water on these acid sites of comparable strength.

Since the starting substances α-AlF_3 and β-AlF_3 also contain traces of oxide/hydroxide (see Table 3), there is always a slight amount of water as a result of the F/OH exchange during the activation present in the system.

CONCLUSIONS

It was the aim of our investigations to obtain information (mainly by ESCA) about the catalytically active aluminum compounds in the surface. With the exception of one compound, all the investigated phases were only able to catalyze the model reaction if an activation with the haloalkane was previously carried out.

Only predried β-AlF_3 offers full activity without activation. XRD and IR reveal no alteration of this phase, and ESCA confirms this result for the sample surface. Therefore a solid phase has been found which is immediately ready for catalysis while other phases must be modified by activation.

As a result of the activation of the samples β-AlF_3–625 K–$CHClF_2$, $AlF_2(OH)$–625 K–$CHClF_2$ and after long-time activation of the sample γ-Al_2O_3–525 K–CH_3CClF_2 surface phases are obtained having similar positions in the chemical state plots, offering comparable F/Al and O/Al atomic percentage ratios, and having almost identical O 1*s* spectra. There is thus a strong correlation between the existence of this special surface phase and the catalytic activity of the respective sample. The structure of these surface phases cannot be determined by XRD, but it is reasonable to assume a short-range order and bonding conditions very similar to those met with in β-AlF_3. A long-range order is unimportant for the heterogeneous

catalysis in any case. The surface composition of the active catalytic phase is similar to β-AlF_3, but the exact surface structure is not entirely clear.

Solid-state reactions in the bulk (also in the absence of haloalkanes) occur above 825 K, for example the decomposition of $AlF_2(OH)$ forming β-AlF_3 and amorphous oxides (5). Under appropriate temperature conditions these bulk processes still do not occur.

A conclusion of previous work was that the surface sites responsible for enabling the catalysis are Lewis acid coordination vacancies near aluminum cations (3, 12). A certain structure is favoured if it possesses suitable geometrical possibilities to enter these sites and if it offers a large number of centers of sufficient strength. The catalytically active phase β-AlF_3 evidently meets these preconditions. This structure has a special AlF_6 octahedral linking with hexagonal hollow tubes (4). Measurements of temperature-programmed desorption of ammonia on β-AlF_3 (12) reveal that this sample adsorbs the largest amount of ammonia per unit surface area compared with the other samples.

The pyrochlore structure ($AlF_2(OH)$) also possesses such hollow tubes, but they are partially occupied by water. The compounds of this structure must be dehydrated and a F/OH exchange must take place. Only after these measures are they catalytically active. The short-range order on the surface of the modified sample is similar to that of β-AlF_3.

In contrast, the pure α-AlF_3 high-temperature phase consisting of universally regular linked octahedra is catalytically inactive. Previous studies (13) show the resistance of this phase. Under appropriate conditions a chemical or structural modification of α-AlF_3 is not possible.

ACKNOWLEDGMENTS

We are grateful to Fonds der Chemischen Industrie and Deutsche Forschungsgemeinschaft for financial support.

REFERENCES

1. Kemnitz, E., and Hess, A., *J. Prakt. Chem.* **334,** 591 (1992).
2. Kauschka, G., and Kolditz, L., *Z. Chem.* **16,** 377 (1976).
3. Hess, A., and Kemnitz, E., *Appl. Catal. A: General* **82,** 247 (1992).
4. Le Bail, A., Jacoboni, C., Leblanc, M., De Pape, R., Duroy, H., and Fourquet, J. L., *J. Solid State Chem.* **77,** 96 (1988).
5. Menz, D.-H., Mensing, C., Hönle, W., and von Schnering, H. G., *Z. Anorg. Allg. Chem.* **611,** 107 (1992).
6. Hess, A., and Kemnitz, E., *J. Mol. Cat.*, in press.
7. Fresenius, W., and Jander, S., "Handbuch der analytischen Chemie," p. 177. Springer-Verlag, Berlin, 1959.
8. Anthony, M. T., and Seah, M. P., *SIA, Surf. Interface Anal.* **6,** 94 (1984).
9. Scofield, J. H., *J. Electron. Spectrosc. Relat. Phenom.* **8,** 129 (1976).
10. Kerkhof, F. P. J. M., and Moulijn, J. A., *J. Phys. Chem.* **83,** 1612 (1979).
11. NIST Standard Reference Database 20 (NIST X-ray Photoelectron spectroscopy Database), Version 1.0, Data compiled and evaluated by C. D. Wagner (NIST Gaithersburg, 1989).
12. Hess, A., and Kemnitz, E., *J. Cat.*, in press.
13. Hess, A., Diplomarbeit, Humboldt-Universität zu Berlin, 1991.
14. Fourquet, J. L., Riviere, M., Le Bail, A., Nygrens, M., Grins, J., *Eur. J. Solid State Inorg. Chem.* **25,** 535 (1988).
15. Wagner, C. D., and Joshi, A., *J. Electron. Spectrosc. Relat. Phenom.* **47,** 283 (1988).
16. Wagner, C. D., Passoja, D. E., Hillary, H. F., Kinisky, T. G., Six, H. A., Jansen, W. T., and Taylor, J. A., *J. Vac. Sci. Technol.* **21,** 933 (1982).
17. Haverkamp, R. G., Metson, J. B., Hyland, M. M., and Welch, B. J., *SIA, Surf. Interface Anal.* **19,** 139 (1992).
18. McGuire, G. E., Schweitzer, G. K., and Carlson, Th. A., *Inorg. Chem.* **12,** 2450 (1973).
19. Lindsay, J. R., Rose, H. R., Swartz, W. E., Watts, Ph. H., and Rayburn, K. A., *Appl. Spectrosc.* **27,** 1 (1973).
20. Taylor, J. A., *J. Vac. Sci. Technol.* **20,** 751 (1982).
21. Strohmeier, B. R., Leyden, D. E., Field, R. S., and Hercules, D. M., *J. Catal.* **94,** 514 (1985).
22. Ng, K. T., and Hercules, D. M., *J. Phys. Chem.* **80,** 2095 (1976).
23. Castle, J. E., and West, R. H., *J. Electron. Spectrosc. Relat. Phenom.* **16,** 195 (1979).
24. Nefedov, V. I., Buslaev, Y. A., and Kokunev, Y. U., *Zh. Neorg. Khim.* **19,** 1166 (1974).
25. Wagner, C. D., *in* "Handbook of X-Ray Photoelectron Spectroscopy." Perkin–Elmer Corp., Physical Electronics Div., Eden Prairie, MN, 1979.
26. Clark, D. T., and Peeling, J., *J. Polym. Sci.* **14,** 2941 (1976).
27. Palchan, I., Crespin, M., Estrade-Szwarckopf, H., and Rousseau, B. *Chem. Phys. Lett.* **157,** 321 (1989).
28. Wagner, C. D., *Faraday Discuss. Chem. Soc.* **60,** 291 (1975).
29. Thomas, T. D., *J. Electron. Spectrosc. Relat. Phenom.* **20,** 117 (1980).
30. Moretti, G., and Porta, P., *SIA, Surf. Interface Anal.* **15,** 47 (1990).
31. α-AlF_3: Al–F = 1.76 Å; Ketelaar, J. A. A., *Nature (London)* **128,** 303 (1930); β-AlF_3: Al–F = 1.880 Å; Le Bail, A., Jacoboni, C., Le Blanc, M., de Pape, R., Duroy, H., and Fourquet, J. L., *J. Solid State chem.* **77,** (1988); 96 Water free Al hydroxyfluoride: $Al–O_{OH}$, F = 1.841 Å, hydrated Al hydroxyfluoride: $Al–O_{OH}$, F = 1.860 Å; see Ref (14) above. $Al(OH)_3$, bayerite: $Al–O_{OH}$ = 1.86 Å; Zigan, F., Joswig, W., and Burger, N., *Z. Kristallogr., Kristallgeom., Kristallphys., Kristallchem.* **148,** 255 (1978). α-Al_2O_3: Al–O = 1.86 Å; L. Lutterotti and P. Scardi, *J. Appl. Crystallogr.* **23,** 246 (1990). This value should be a good approximation for the situation in γ-alumina.
32. Thomson, J., Webb, G., and Winfield, J. M., *J. Chem. Soc., Chem. Commun.* **5,** 323 (1991).
33. Wandelt, K., *Surf. Sci. Rep.* **2,** 1 (1982).